

A quantum register using collective excitations in an atomic ensemble without a Rydberg blockade

Elisha Haber,^{1,2,*} Zekai Chen,^{1,2,†} and Nicholas P. Bigelow^{1,2,3}

¹*Department of Physics and Astronomy, University of Rochester, Rochester, New York 14627, USA*

²*Center for Coherence and Quantum Optics, University of Rochester, Rochester, New York 14627, USA*

³*The Institute of Optics, University of Rochester, Rochester, New York 14627, USA*

(Dated: November 18, 2022)

A qubit made up of an ensemble of atoms is attractive due to its resistance to atom losses, and many proposals to realize such a qubit are based on the Rydberg blockade effect. In this work, we instead consider an experimentally feasible protocol to coherently load a spin-dependent optical lattice from a spatially overlapping Bose–Einstein condensate. Identifying each lattice site as a qubit, with an empty or filled site as the qubit basis, we discuss how high-fidelity single qubit operations, two-qubit gates between arbitrary pairs of qubits, and nondestructive measurements could be performed. In this setup, the effect of atom losses has been mitigated, and we never need to remove the atoms from the computational basis in the ground state manifold, both of which can be significant sources of decoherence in other types of atomic qubits.

I. INTRODUCTION

Quantum computers are of interest primarily because they could be used to efficiently solve problems that would be intractable on a classical computer [1]. One promising candidate for a scalable quantum computer researchers have been pursuing is trapped neutral atoms, and there have been many proposals for how to realize qubits using cold atoms [2–5]. In optical lattices, or arrays of microtraps, one or more atoms are confined in individual traps, and the spatial [6, 7] or spin [2, 3, 8] state of the atom(s) is used to define the qubit. Qubits made up of multiple atoms are more resistant to atom losses and require lower Rabi frequencies, but gate operations can be more difficult due to the qubits not being identical to each other, or even the same between realizations [9–11].

Two-qubit gates in lattices can be realized by bringing different qubits close together [3, 12, 13], mediating the interaction using a quantum bus (such as an optical cavity [14, 15] or spin chain [16]), or by using the dipole-dipole interaction between distant Rydberg atoms [14, 17–20]. Qubit gates based on shuttling atoms around or using spin chains are often slower, whereas the Rydberg and optical cavity approaches are faster, but can be prone to a greater variety of errors.

Measurements in lattice-based qubits are usually based on resonant absorption or fluorescence in high-resolution optical imaging systems [21–24]. Such approaches allow each qubit to be measured with very high accuracy, but can cause heating.

Researchers have also considered realizing cold atom qubits using Bose–Einstein condensates (BECs) [25–29],

often analogously to their superconducting Josephson junction counterparts. Although these platforms may be less scalable and suffer from longer gate times compared to lattice-based approaches, it can be easier to read out their states without using resonant light because BECs are mesoscopic objects [30–34]. Additionally, it can be easier to couple BECs (rather than single atoms) to photonic flying qubits [35].

In this work, we consider realizing a quantum register using a BEC in a harmonic trap, and a spatially overlapping spin-dependent optical lattice. The proposed system is nearly identical to those of [36–38]. The goal is to combine the scalability and qubit connectivity of lattice-based platforms with the resistance against atom losses and nondestructive readout available on BEC-based ones. We begin by discussing the experimental setup in section II, our Hamiltonian in section III, how single and two-qubit gates can be realized in sections IV and V, respectively, and how nondestructive qubit measurements could be performed in section VI.

II. THE SETUP

It is assumed that we begin with a BEC of N ^{87}Rb atoms in the $5^2\text{S}_{1/2}$ ground state manifold Zeeman sublevel $|F, m_F\rangle = |1, 0\rangle$. The atoms are confined to a 3D nearly-harmonic optical dipole trap (HO), of trapping frequency ω_{HO} , by a pair of perpendicularly propagating Gaussian beams [39].

A 3D spin-dependent lattice (OL) may be formed by intersecting three pairs of nearly counterpropagating, linearly polarized beams where one beam in each pair has had its polarization vector rotated by an angle θ with respect to the polarization vector of the other beam (see Fig. 1). The dipole potential of the OL will then be [36]

* Corresponding author: ehaber@ur.rochester.edu

† Current address: Institut für Experimentalphysik und Zentrum für Quantenphysik, Universität Innsbruck, 6020 Innsbruck, Austria

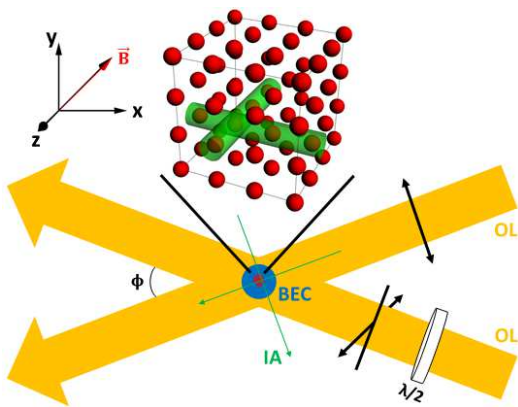


FIG. 1. Experimental setup. The pair of OL beams that create the lattice potential along the x-axis are shown intersecting at an angle, ϕ . One beam passes through a half-wave plate and has its polarization vector rotated by $\theta = 90^\circ$. The dilute BEC, which does not see the OL beams, is shown in blue, while the atoms that do see the lattice potential are shown in red. The two tightly focused IA beams that individually address atoms in the lattice are shown in green.

$$V(\mathbf{r}) = \frac{\pi c^2 I_0 \Gamma}{\omega_0^3} \left\{ \left(\frac{2}{\Delta_2} + \frac{1}{\Delta_1} \right) (1 + \cos(\theta) \cos(2\mathbf{k} \cdot \mathbf{r})) + g_F m_F \left(\frac{1}{\Delta_2} - \frac{1}{\Delta_1} \right) (\hat{\mathbf{k}} \cdot \hat{\mathbf{B}}) \sin(\theta) \sin(2\mathbf{k} \cdot \mathbf{r}) \right\}, \quad (1)$$

where I_0 is the beam intensity, Γ is the spontaneous emission rate of the excited state, ω_0 is the transition frequency, $\Delta_{1,2}$ are the laser detunings from the ^{87}Rb D_1 and D_2 lines respectively, \mathbf{k} is the wavevector of the beam, $|\mathbf{k}| = 2\pi/\lambda$, λ is the beam's wavelength, and \mathbf{B} is the (homogenous) magnetic field.

If we choose $\theta = 90^\circ$, then by Eq. (1) only atoms in the $m_F \neq 0$ Zeeman sublevels will see the lattice beams (see Fig. 2). With this setup, reasonable optical powers require λ near the ^{87}Rb D_1 and D_2 lines. We set $\lambda = 790$ nm because, at this wavelength, atoms in $m_F = 0$ will not see the lattice beams even with imperfect polarization. The effective lattice spacing is given by $\lambda/2 \sin(\phi)$, where ϕ is the angle at which the lattice beams intersect [36]. $\phi = 48^\circ$ yields an effective lattice spacing of 532 nm, which is sufficient to allow the lattice sites to be individually addressed using tightly focused optical (IA) beams [40], although alternative approaches also exist [41]. For $\lambda/2 \sin(\phi) < \sqrt{\hbar/m\omega_{\text{HO}}}$ the lattice sites will be concentrated near the bottom of the harmonic trap (see the different length scales in Fig. 2). \mathbf{B} is oriented so that its components along the three lattice axes are equal.

We use the number of atoms in each lattice site as a qubit, and label an empty site as the qubit level $|\downarrow\rangle$, and a site with one atom as the qubit level $|\uparrow\rangle$. Defining the computational basis in this way protects our qubits against the usually destructive nature of atom losses, and

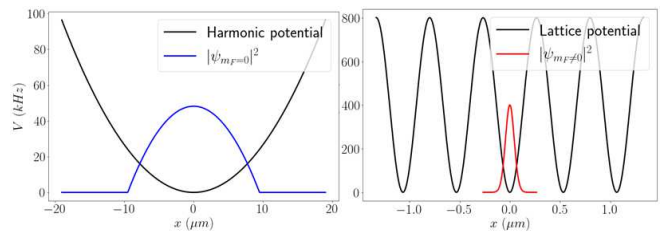


FIG. 2. Harmonic and spin-dependent lattice potentials along the x-axis. In the proposed setup, atoms with $m_F = 0$ will only see the nearly harmonic Gaussian potential, while atoms with $m_F \neq 0$ will also see the lattice potential. The probability densities for the atoms in each state are shown by the red and blue curves.

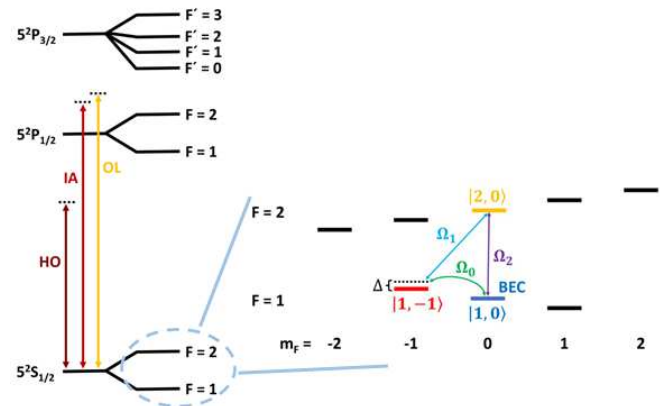


FIG. 3. ^{87}Rb level spectrum. The HO, OL, and IA beams are shown with optical wavelengths far-detuned from the D_1 line. Ω_0 is an RF field shown connecting the two qubit levels, while Ω_1 and Ω_2 are MW fields that are used to entangle qubits together and to perform measurements. Δ is the detuning of the Ω_0 and Ω_1 fields from resonance.

if the the number of qubits in our register, n , is much less than N , then this will also greatly extend the energy relaxation time of the qubits (see App. C). Finally, this allows us to avoid needing to load exactly one atom into each lattice site to initialize the qubits [42–44].

One disadvantage that arises from this choice of qubit states is that the transition frequency will be sensitive to fluctuations in both the magnetic field, and the intensities of the lattice beams (see App. B). We suggest ways to mitigate this shortcoming in App. D, and note there are many general methods for doing so [45–49].

III. THE HAMILTONIAN

To model our system, we start with the second quantized Hamiltonian for interacting bosonic atoms [26, 50],

$$\begin{aligned}
\hat{H} = & \sum_i \int d\mathbf{r} \hat{\psi}_i^\dagger(\mathbf{r}) \left(-\frac{\hbar^2}{2m} \nabla^2 + V_i(\mathbf{r}) + \hbar\omega_i \right) \hat{\psi}_i(\mathbf{r}) \\
& + \sum_{i,j} \int d\mathbf{r} d\mathbf{r}' \hat{\psi}_i^\dagger(\mathbf{r}) \hat{\psi}_j^\dagger(\mathbf{r}') U_{ij}(\mathbf{r}, \mathbf{r}') \hat{\psi}_i(\mathbf{r}) \hat{\psi}_j(\mathbf{r}') \\
& - \sum_{i \neq j} \int d\mathbf{r} \left(\hbar\Omega_{ij}(\mathbf{r}, t) \hat{\psi}_i^\dagger(\mathbf{r}) \hat{\psi}_j(\mathbf{r}) + \text{h.c.} \right), \quad (2)
\end{aligned}$$

where the sums are performed over all states in the $5^2S_{1/2}$ manifold, $\hat{\psi}_i(\mathbf{r})$ is the bosonic field operator for atoms in state i , $V_i(\mathbf{r})$ is the external potential for atoms in i , $\hbar\omega_i$ is the energy of the atom's internal state, U_{ij} is the two-body interaction potential for any pair of atoms, $\Omega_{ij}(\mathbf{r}, t)$ is the Rabi frequency of the field connecting states i and j , and h.c. denotes the Hermitian conjugate.

The first term in Eq. (2) is the single-particle Hamiltonian, the second accounts for intra- and interparticle interactions, and the last term allows for transitions between the atomic levels due to the microwave (MW) and radiofrequency (RF) fields. It has been assumed that a background magnetic field is present that allows us to ignore spin-exchange collisions [51].

For atomic states with $m_F = 0$, $V_i(\mathbf{r})$ is given by a 3D isotropic Gaussian function, while for states with $m_F \neq 0$ $V_i(\mathbf{r})$ is given by Eq. (1). The two-body interaction potential in Eq. (2) is given by [52, 53]

$$U_{ij}(\mathbf{r}, \mathbf{r}') = \frac{4\pi\hbar^2 a_{ij}}{m} \delta(\mathbf{r} - \mathbf{r}') \left(1 - \frac{\delta_{ij}}{2} \right), \quad (3)$$

where $i, j = (F, m_F)$, (F', m'_F) , a_{ij} is the s-wave scattering length for the pair of atoms, and m is the mass of each atom. The scattering lengths for all combinations of spins were calculated with the methods and numbers in [52–54], and the results are given in App. A.

For atoms in states with $m_F = 0$, we assume that N is large enough that we can make the Thomas-Fermi (TF) approximation in calculating $\hat{\psi}_i(\mathbf{r})$ [55, 56]. For atoms in all other states, the interactions are weak enough that the $\hat{\psi}_i(\mathbf{r})$ can be expanded in the basis of the single particle solutions, which are Bloch wavefunctions for atoms in a lattice [57]. If the trap frequencies are the largest energy scale in the problem, then we may restrict our attention to the lowest Bloch band and expand $\hat{\psi}_i(\mathbf{r})$ in the Wannier basis. Additionally, we assume that the lattice is deep enough that tunneling and interactions between atoms in different sites may be neglected (see App. A).

Plugging Eq. (3) into Eq. (2) and integrating then yields the Bose-Hubbard Hamiltonian [57, 58],

$$\begin{aligned}
\hat{H} = & \sum_{s,i} \left(\frac{1}{2} U_{si}^{si} \hat{n}_{si} (\hat{n}_{si} - 1) + \sum_{r \neq s,j} U_{si}^{rj} \hat{n}_{si} \hat{n}_{rj} \right) \\
& + \sum_{s,i} \left(\epsilon_{si} \hat{n}_{si} - \sum_{r \neq s,j} \hbar \left(\Omega_{si}^{rj}(t) \hat{a}_{si}^\dagger \hat{a}_{rj} + \text{h.c.} \right) \right), \quad (4)
\end{aligned}$$

where the sums are performed over all the spin states and lattice sites, s, r denote the atomic spin states, i, j denote the spatial eigenstates of the atoms, U_{si}^{rj} is the interaction strength between an atom in state s, i and one in r, j , $\hat{n}_{si} = \hat{a}_{si}^\dagger \hat{a}_{si}$, \hat{a}_{si}^\dagger is the creation operator for atoms in state s, i , ϵ_{si} is the total energy of an atom in state s, i , and Ω_{si}^{rj} is the Rabi frequency for a transition between states s, i and r, j , which is approximately given by a Franck-Condon-like factor [58],

$$\Omega_{si}^{rj}(t) = \int d\mathbf{r} \psi_{si}^\dagger(\mathbf{r}) \tilde{\Omega}_{si}^{rj}(\mathbf{r}, t) e^{-i\mathbf{k} \cdot \mathbf{r}} \psi_{rj}(\mathbf{r}), \quad (5)$$

where $\psi_{si}(\mathbf{r})$ is the spatial wavefunction for atoms in state s, i , $\tilde{\Omega}_{si}^{rj}(\mathbf{r}, t)$ is the Rabi frequency for the transition if the atoms were in free space, and \mathbf{k} is the wavevector of the field. We will make the rotating-wave approximation (RWA) throughout the paper to make Rabi frequencies time independent. The field frequencies will always be chosen to cancel (to within experimental error) the energies of the two states we wish to connect.

IV. SINGLE QUBIT OPERATIONS

Single qubit gates may be implemented using the Hamiltonian given by Eq. (4). We consider using tightly focused (0.6 μm radius), 790.02 nm wavelength IA beams to shift the energy difference between the qubit state $|1, -1\rangle$ and the BEC state $|1, 0\rangle$ (see App. A for all of the numbers used in our calculations). In [59], it was shown that qubit operations on individual lattice sites of a 3D lattice could be done using a pair of IA beams. According to Eq. (1), for pure circular polarization, the BEC atoms will not see any light shift at this ‘magic’ wavelength.

To turn on Rabi flopping between the qubit states, we apply a spatially-uniform RF field that is resonant with the transition $|1, 0\rangle \rightarrow |1, -1\rangle$ (see Fig. 3). If the background magnetic field is large enough then the quadratic Zeeman shift will allow us to drive the $|1, 0\rangle \rightarrow |1, -1\rangle$ transition without also driving $|1, 0\rangle \rightarrow |1, 1\rangle$.

The Rabi frequency for this transition, Ω_0 , is calculated with Eq. (5), where ψ_{si} is the TF wavefunction for the BEC and ψ_{rj} is the Wannier function for the lattice site that is being addressed. For the experimental parameters considered in App. A, the overlap integral in Eq. (5), for the lattice sites farthest from the center of the trap, is $1/364$. After taking into account the \sqrt{N} bosonic enhancement that comes from coupling to the BEC, this leads to an effective Rabi frequency of ~ 2.30 times the free space Rabi frequency.

We obtain $\Omega_0 = 2\pi \times 100$ Hz, a π -pulse time of 5.03 ms, and an estimated error rate below 0.001 (see App. B). The gate speed is primarily limited by the requirement that $\Omega_0 \ll U/\hbar = 13.0$ kHz, where U is the interaction strength between atoms in the same lattice site, which is needed to avoid loading multiple atoms into the same site.

V. ENTANGLING QUBITS

In this section, we consider using the BEC as a native quantum bus to entangle distant pairs of atoms and realize a CNOT gate. This does not require the qubit atoms be shuttled around [3, 12], brought outside the qubit basis [18], or extra optics [15]. We also show how to implement a $\sqrt{\text{SWAP}}$ gate in App. F.

The first step of the protocol is to transfer $1/5$ of the BEC population from $|1, 0\rangle$ to $|2, 0\rangle$ using the MW field Ω_2 . One qubit in our array is addressed by the IA beams and then entangled with the BEC by driving the virtual two-photon transition shown in Fig. 3 with the fields Ω_0 and Ω_1 . This will cause the population of $|2, 0\rangle$ to be a function of whether the qubit is in $|\uparrow\rangle$ or $|\downarrow\rangle$.

If the qubit is in $|\uparrow\rangle$, then there will be a blockade effect and the populations of $|1, 0\rangle$ and $|2, 0\rangle$ will not change. If the qubit was in $|\downarrow\rangle$, then the population of $|2, 0\rangle$ will oscillate between $N/5$ and $4N/5$ (see App. E). The Ω_0 and Ω_1 fields are turned off once the population reaches $4N/5$. The qubit state will be left unchanged provided $\Delta \gg \Omega_0, \Omega_1$. Note that initially loading some of the population from $|1, 0\rangle$ into $|2, 0\rangle$ is necessary to prevent coupling between the intermediate Wannier state and the excited spatial levels of the harmonic trap during this process.

Next, we entangle a second qubit with the BEC using the same technique described in section IV. Ω_0 alone is turned on with $\Delta = 0$, and the IA beams are centered on a second qubit in the array. The second qubit will undergo Rabi oscillations at a frequency proportional to the square root of the number of atoms in $|1, 0\rangle$. Thus, these oscillations will be half as fast if the first qubit is in $|\uparrow\rangle$. After a π -pulse, the second qubit will have had its state flipped only if the first qubit was in $|\uparrow\rangle$. Lastly, the BEC bus must be reset.

This sequence of pulses thus realizes a CNOT gate, which, together with arbitrary single qubit operations, forms a universal gate set [1, 60]. Using the parameters given in App. A, the estimated gate time is ~ 28 ms, which was computed using two qubits that are maximally separated ($\sim 8 \mu\text{m}$ apart). The time is primarily limited by the virtual transition step, which is slow due to the small overlap between the TF and Wannier wavefunctions. Reducing the gate time would require free space Rabi frequencies > 1 MHz. Another limitation is that the CNOT gate can not be performed on multiple pairs of qubits in parallel (we note that the two-qubit protocol in App. F does not have this drawback).

VI. NONDESTRUCTIVE READOUT

We propose a method to read out the state of any individual qubit in our array by coupling the qubit to the BEC, and then nondestructively measuring the BEC state. Following the protocol given in section V, $1/5$ of the BEC population is first transferred from $|1, 0\rangle$ to

$|2, 0\rangle$ using the MW field Ω_2 . Then, Ω_0 and Ω_1 are used to drive population between these levels, which will be successful if and only if the qubit is in $|\downarrow\rangle$.

There are several methods to nondestructively detect population oscillations in a BEC. It was shown in [30] that Rabi oscillations between the two $m_F = 0$ levels in ^{87}Rb atoms may be observed by measuring the MW impedance of the atoms. In Ref [33], BEC atoms coherently exchanged photons with two optical beams, and the resulting intensity fluctuations in the beams were observed on a CCD camera.

Compared to more conventional measurement approaches [21–23], in the one proposed here there is little chance of the qubit atoms being heated or lost during the imaging process, and no high-resolution optics are required. However, only one qubit can be measured at a time, and there will be decoherence introduced to the BEC during readout. We note that the system is also compatible with the usual fluorescence-based approaches.

VII. CONCLUSION

We propose to use a 3D spin-dependent optical lattice as a quantum register, and a spatially overlapping BEC as a reservoir of atoms. Single qubit operations are realized by loading single atoms from the BEC into lattice sites. By coupling the qubits to the BEC, we show how a CNOT gate could be implemented between arbitrary pairs of qubits without either qubit being brought outside of the computational basis. Lastly, we discuss how non-destructive measurements could be carried out without heating up the atoms.

Compared to Rydberg-based qubits, this platform has slower gate times and computational states that have greater sensitivity to fluctuations in the magnetic field and lattice beams. However, the qubits are much better protected against decoherence due to atom losses, never need to be taken out of the computational basis, are fully connected, and can be measured nondestructively without additional heating of the atoms.

The proposed system represents a new pathway for achieving quantum computers using neutral atoms, which attempts to address many of the problems currently facing cold atom-based qubits, and there is much research still to be done. Work on addressing individual qubits without the need for any tightly focused optical beams by phase imprinting topological defects in the BEC, and using the BEC to probe changing experimental parameters so that computation errors may be corrected in real-time, is already underway. In the future, we hope to experimentally realize this system and demonstrate its potential to push the field forward.

VIII. ACKNOWLEDGMENTS

We would like to thank Maitreyi Jayaseelan, Joseph D. Murphree, and Nathan Lundblad for helpful conversations. This work was supported by NSF grant PHY 1708008, NASA/JPL RSA 1656126.

Appendix A: Experimental implementation

In this section, we give realistic experimental parameters that could be used to realize the system considered in the main text. We assume that we begin with an ultracold cloud of 10^6 ^{87}Rb atoms at $T = 300$ nK. At this temperature, the BEC fraction will be about 70%, which means we should have $N = 7 \times 10^5$ BEC atoms in the trap. A small background magnetic field is only necessary to define a quantization axis, so we assume a small steady field is present at all times.

We consider a 3D isotropic harmonic dipole trap formed by crossed $\lambda = 808$ nm beams. Both HO beams are linearly polarized and have beam powers of 100 mW. One beam has beam waists of 120 μm and 90 μm , while the other has 132 μm and 87.3 μm . These yield a harmonic trapping frequency of $\omega_{\text{HO}} = 2\pi \times 100$ Hz.

The IA beams used to address individual lattice sites have $\lambda = 790.02$ nm with beam waists of 0.6 μm and circular polarization.

The 3D optical lattice is formed by 3 pairs of nearly counterpropagating $\lambda = 790$ nm beams, which intersect at an angle of $\phi = 48^\circ$. All OL beams are linearly polarized, and one beam in each pair has had its polarization vector rotated by $\theta = 90^\circ$. Each beam has a beam power of 67 mW, and a beam waist of 150 μm in each direction.

If we label the following states $|0\rangle = |1, 0\rangle$, $|1\rangle = |1, -1\rangle$, and $|2\rangle = |2, 0\rangle$, then the scattering lengths between all pairs of states are $a_{00} = 5.34$ nm, $a_{11} = 5.31$ nm, $a_{22} = 5.00$ nm, $a_{01} = 5.31$ nm, $a_{02} = 5.23$ nm, and $a_{12} = 5.16$ nm. For the lattice parameters considered above, lattice depth will be 800 kHz, the spacing 532 nm, the interaction energy between two atoms in the same site 13 kHz, the tunneling energy 0.09 Hz, and the separation between the first and second Bloch bands will be 190 kHz. We restrict our attention to the $n = 10 \times 10 \times 10$ lattice sites closest to the trap center.

For single qubit gates involving atoms farthest from the center of the trap (i.e. the atoms with the longest gate time), the free space Rabi frequency $\tilde{\Omega}_0 = 2\pi \times 43.5$ Hz is considered. With a detuning of -9.96 kHz from atomic resonance, the effective Rabi frequency will be $\Omega = 2\pi \times 100$ Hz, the two states we are trying to connect will be approximately degenerate after the RWA, and thus the π -pulse time will be 5.03 ms.

For the two-qubit CNOT gate's initial MW pulse, the Rabi frequency is $\Omega_2 = 2\pi \times 159$ kHz with no detuning. This yields a pulse time of 0.464 ms. For the two-photon process on atoms farthest from trap center, the free space single-photon Rabi frequency is $2\pi \times 160$ kHz,

and the single-photon detuning is 13 kHz. The effective two-photon Rabi frequency will be $2\pi \times 18$ Hz, and the pulse time 11.1 ms. The next step is identical to the single qubit gate, and lastly the BEC bus needs to be reset, which leads to a total CNOT gate time of ~ 28 ms.

Appendix B: Sources of decoherence

There are many sources of decoherence in this approach, and several are discussed here. For each source of error, we estimated either the probability of a qubit leaving the computational basis, or the uncertainty it would introduce into the Rabi frequencies or qubit levels. In all cases, we roughly estimate the error rates by assuming that all of the noise sources are independent and follow Gaussian distributions. For each source of error, we sample the distribution and find that the resulting error rate on the qubit operations is below 0.001.

We first look at reasons why multiple atoms could occupy the same lattice site. For a deep optical lattice, there will be strong s-wave interactions between atoms in the same site, $U_{\text{si}}^{\text{si}}/\hbar = 13.0$ kHz. We therefore require $\hbar\Omega_0 < U_{\text{si}}^{\text{si}}$ to avoid double occupation of the lattice site during single qubit operations. If two atoms share a lattice site then they will most likely collide and both be ejected from the trap within one millisecond [61, 62]. If the second atom came from the BEC or background gas, then this process maps $|\uparrow\rangle \rightarrow |\downarrow\rangle$. If the second atom came from another lattice site, then this maps $|\uparrow\uparrow\rangle \rightarrow |\downarrow\downarrow\rangle$. Tunneling between lattice sites could be suppressed by using a deeper lattice, or by utilizing the gravitational field, applying a magnetic field gradient, or accelerating the lattice so that the atoms will see a potential gradient [63].

Using the BEC to mediate qubit operations will also introduce noise into the system. We require $N \gg 10^3$, or the \sqrt{N} shot-to-shot fluctuations in N will significantly change the effective Rabi frequency for coupling between lattice atoms and the BEC. N must also be much greater than the number of noncondensed atoms, or the coupling between $|1, -1\rangle$ and the noncondensed atoms will not be negligible. When accounting for the noncondensed atoms, we followed the heuristic approach of [56] and assumed that the density of the noncondensed atoms is just the TF density with an appropriate scaling factor. Finally, we require $N \gg n$ or the pulse time for each qubit will be influenced by the states of all other qubits.

There will be uncertainty in the qubit transition frequency for several reasons. Interaction between the $N \pm \sqrt{N}$ BEC atoms and the lattice atoms introduces ~ 28.7 Hz uncertainty in the difference between the levels. Fluctuations in the magnetic field (± 4.3 nT [64]) leads to ~ 30 Hz uncertainty due to the Zeeman effect. Fluctuations in the lattice beam intensities (± 312 mW/cm²) yield ~ 28 Hz uncertainty, and an error in the rotation of the lattice beam's polarization vector, θ , by $\pi/150$ will introduce an uncertainty of ~ 11.2 Hz. Reduc-

ing the effect of the background BEC on the qubit transition frequency could be done by decreasing the BEC density, but this would also decrease the gate speed. Methods to suppress the effects of magnetic field and lattice beam intensity fluctuations are discussed in App. D.

We must also have $\Omega_{0,1}$ much smaller than both the frequency difference between the first and second lattice bands (190 kHz) to avoid populating higher Bloch bands. Population of $|1, 1\rangle$ during single qubit operations will be suppressed by the differential Zeeman effect, and because atoms in $|1, 1\rangle$ will see a lattice that is 180° out of phase with the lattice potential seen by atoms in $|1, -1\rangle$.

For two-qubit gates, after the population transfer in the first step of the process, the two $m_F = 0$ BEC states' wavefunctions will evolve in time because their TF profiles will no longer be the ground state. To approximate these dynamics, we evolved the spatial wavefunctions of both BEC components in time using a fourth-order Runge-Kutta method to solve the Gross-Pitaevskii equation. We found that, based on this estimate, the spatial dynamics during the gate operation will be negligible.

In order to address individual qubits, the IA beams must shift the energy levels of the qubit to be addressed (relative to its neighbors) by an amount much greater than the Rabi frequency [40, 59]. The lattice will slowly drift over time, which is a problem both for centering the IA beams on specific lattice sites, as well as for computing the interaction and coupling strengths between individual lattice sites and the background BEC, the last two of which are problems unique to our approach. Here we assume that, with a proper feedback system, the lattice position can be stabilized to within $0.1\lambda/2$ [40, 65]. The BEC has a TF radius of $18.1 \mu\text{m} \gg \lambda$. Consequently, we find that the effects of the uncertainty in the lattice position on coupling to the BEC during gate operations should be far below the 0.001 threshold.

Appendix C: Atom losses

Each of the N atoms that were initially in the harmonic trap is equally likely to occupy the lattice site of each qubit that is in $|\uparrow\rangle$. Following the approach in [9], when $k < N$ atoms are lost from the system the probability that a lattice atom was lost can be found by calculating the ratio between the number of states in which at least one lattice atom was lost, and the total number of states. For simplicity, a definite number of qubits, $m \leq n$, are assumed to be in state $|\uparrow\rangle$. We denote the (unnormalized) state of the N atoms as

$$|12\dots m00\dots 0\rangle + |12\dots 0m0\dots 0\rangle + \dots |00\dots 012\dots m\rangle, \quad (\text{C1})$$

where $1, 2, \dots, m$ denote which lattice site that atom is in, and 0 denotes that the atom is in the harmonic trap. We observe that there are a total of $P(N, m)$ states in the superposition given by Eq. (C1) (where $P(N, m)$ denotes m -permutations of N).

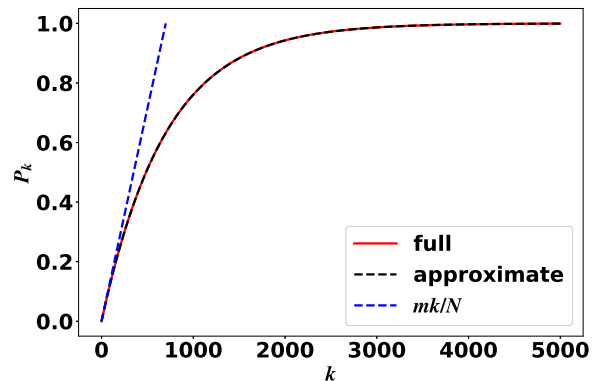


FIG. 4. Probability of a bit flip occurring as a function of the number of lost atoms. The curve labeled 'full' corresponds to Eq. (C2), and 'approximate' to Eq. (C3). $N = 7 \times 10^5$ atoms and $m = 1,000 |\uparrow\rangle$ qubits were used to generate the plot.

We consider what happens, without loss of generality, when the first $k < N$ atoms are lost. In $P(N - k, m)$ states the first k atoms do not carry any quantum information. Thus, the probability of at least one lattice atom being lost will be given by

$$P_k = 1 - \frac{P(N - k, m)}{P(N, m)} = 1 - \prod_{j=0}^{m-1} \left(1 - \frac{k}{N - j}\right). \quad (\text{C2})$$

For $N \gg m$,

$$P_k \approx 1 - \left(1 - \frac{k}{N}\right)^m. \quad (\text{C3})$$

For $k \ll N$ we have $P_k \approx mk/N$, where mk/N is the expected number of compromised qubits after k losses.

P_k is plotted in Fig. 4 using the parameters given in App. A. We observe that, compared to platforms where each qubit is made up of a single atom, in the proposed scheme the quantum register is well protected against atom losses that are much smaller than the size of the ensemble. We also note that, unlike for most cold atom qubits, atom losses do not destroy the qubits here. Instead, atom losses represent an energy relaxation mechanism that results in bit flips $|\uparrow\rangle \rightarrow |\downarrow\rangle$.

In our setup, the magnetic field is large enough that spin-exchange collisions should be negligible [51]. Therefore, the main sources of atom losses are expected to be heating due to the optical lattice and three-body losses in the harmonic trap. For the parameters considered in App. A, we estimate the corresponding lifetimes to be about 4.99 sec due to momentum diffusion in the lattice [36], 0.522 sec due to photon scattering from the lattice beams [39], and 18.3 sec due to three-body losses [66]. We note that techniques to continuously reload a BEC to counter the effects of atom losses have already been experimentally demonstrated [67].

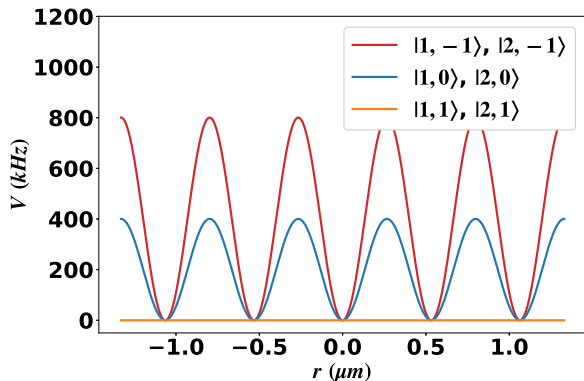


FIG. 5. Lattice potentials used in the method to minimize the influence of magnetic field noise. By adding an extra set of OL beams, which are 180° out of phase with the first set and do not have rotated polarization vectors (but are otherwise identical), atoms in $|1, -1\rangle$ will see a lattice while atoms in $|2, 1\rangle$ will not. Note that the small differences between the potentials seen by atoms with the same values of m_F but different values of F were ignored to generate the plot.

Appendix D: Methods to mitigate fluctuations in the qubit transition frequency

The energy difference between the qubit levels defined in the main text will vary approximately linearly with small fluctuations in the magnetic field and the intensities of the OL beams. In this appendix, we explore two methods to reduce the sensitivity of the transition frequency to these types of noise.

Magnetic field fluctuations are problematic because the BEC state was chosen to be $|1, 0\rangle$, and the lattice state is $|1, -1\rangle$. For the small magnetic field considered here, the splitting between these levels is given by the linear Zeeman effect, $-0.7m_F$ MHz/G. To overcome this limitation we can instead define the BEC state to be $|2, 1\rangle$, while keeping the lattice state as $|1, -1\rangle$. At the "magic" field value $|\mathbf{B}| = 3.229$ G (from the Breit-Rabi formula), the qubit transition frequency will be, to first order, insensitive to fluctuations in $|\mathbf{B}|$.

In order to use $|2, 1\rangle$ as the BEC state, we consider adding a second set of OL beams, with the same wavelength and intensities as the first set described in section II, but with an 180° phase delay and no polarization vector rotation (in Eq. (1), $\theta = 0$ for these beams). The result of this arrangement is that atoms in $|1, -1\rangle$ will see two identical lattices that constructively add together, atoms in $|2, 1\rangle$ and $|1, 1\rangle$ will see two lattices that are 180° out of phase and so they will not experience any net lattice potential, while atoms in $|1, 0\rangle$ and $|2, 0\rangle$ will see a lattice with the same phase and periodicity, but half the height, as the one atoms in $|1, -1\rangle$ see (see Fig. 5). Thus, we may use the $|2, 1\rangle$ and $|1, 1\rangle$ levels as our two BEC states, and $|1, -1\rangle$ as our lattice state.

Single qubit operations will now require a two-photon process where $|2, 0\rangle$ is the intermediate state. If both

sets of beams are derived from the same laser, then relative intensity and phase fluctuations between the beams should be minimal. Absolute intensity fluctuations, however, will still affect the qubit transition frequency.

To protect against intensity fluctuations in the lattice beams, we consider adding a single correction beam that is slightly red-detuned from the ^{87}Rb D_1 line and circularly polarized. If the correction beam's intensity and wavelength are appropriately chosen, and if the intensity fluctuations in the OL and correction beams are coupled, then their effects on the qubit transition frequency will cancel. For the parameters considered in section App. A, small fluctuations in the OL beams will cause fluctuations in the lattice depth, which will cause the qubit transition frequency to change by ~ 0.0898 Hz / (mW / cm 2). For the correction beam, the magic wavelength is $\lambda = 796$ nm. We select an optical power of 3.56 mW and a beam waist of 1 mm, which are chosen so that the beam will be very flat over the region of interest.

If the optical powers of the OL and correction beams are perfectly coupled, then the qubit transition frequency will be, to first order, independent of the precise values of the magnetic field and lattice beam intensities.

Appendix E: Derivation of the dynamics of the two-qubit gate

Here, we describe the derivation of the effective Hamiltonian for the two-photon virtual process given in section V. We begin with the Hamiltonian given by Eq. (4) and restrict our attention to the three atomic states that are colored in Fig. 3: $|1, 0\rangle$, $|1, -1\rangle$, and $|2, 0\rangle$. When Ω_0 and Ω_1 are the only fields on, and $\Delta \gg \Omega_0, \Omega_1$, the energy spectrum will be divided into well-separated manifolds. Each manifold has a different number of atoms in $|1, -1\rangle$, and because Δ is so large the system does not have enough energy to leave the manifold by changing the occupation of $|1, -1\rangle$. If we write the Hamiltonian in the Fock state basis, then we can calculate an effective Hamiltonian that acts only within a given manifold [68].

The goal is to calculate the effective coupling between different states in the same manifold, and the AC Stark shift for each state in our basis. We begin with states of the form $|N_0, 0, N_1\rangle$, where N_0 is the number of atoms in $|1, 0\rangle$, N_1 is the number of atoms in $|2, 0\rangle$, and there are 0 atoms in $|1, -1\rangle$. Up to second order in perturbation theory, the only relevant states are those that are connected to $|N_0, 0, N_1\rangle$ by one or two-photon processes,

$$\begin{array}{l}
 |N_0 + 1, 0, N_1 - 1\rangle \\
 |N_0, 0, N_1\rangle \\
 |N_0 - 1, 0, N_1 + 1\rangle \\
 |N_0, 1, N_1 - 1\rangle \\
 |N_0 - 1, 1, N_1\rangle
 \end{array}
 \begin{pmatrix}
 \omega_0 & & & & \\
 0 & \omega_1 & & & \\
 0 & 0 & \omega_2 & & \\
 \Omega_0 \sqrt{N_0 + 1} & \Omega_1 \sqrt{N_1} & 0 & \omega_3 & \\
 0 & \Omega_0 \sqrt{N_0} & \Omega_1 \sqrt{N_1 + 1} & 0 & \omega_4
 \end{pmatrix},$$

where the $\hbar\omega_i$ are the energies of each Fock state. These terms are computed using Eq. (4) in the RWA (the extra factors of $1/2$ were absorbed into Ω_0 and Ω_1).

We now make several assumptions to obtain the desired behavior. If the single photon detuning, Δ , is much greater than any of the interaction energies except for the interaction energy of two lattice atoms (a condition well satisfied by the choice of experimental parameters in App. A), then we may drop these interaction terms in our calculation of $\omega_{3,4} - \omega_{0,1,2}$. Additionally, we assume that the two-photon detuning is zero, and that the field amplitudes are chosen so that $\Omega_0 = \Omega_1 = \Omega$.

Following [68], we obtain the effective Hamiltonian,

$$\begin{pmatrix} |N_0 + 1, 0, N_1 - 1\rangle \\ |N_0, 0, N_1\rangle \\ |N_0 - 1, 0, N_1 + 1\rangle \end{pmatrix} \begin{pmatrix} \hbar\omega & & \\ \frac{\hbar\Omega^2}{\Delta} \sqrt{N_1(N_0 + 1)} & \hbar\omega & \\ 0 & \frac{\hbar\Omega^2}{\Delta} \sqrt{N_0(N_1 + 1)} & \hbar\omega \end{pmatrix},$$

where $\omega = -\Omega^2(N_0 + N_1)/\Delta$ is the AC Stark shift. Since ω is identical for each state in this manifold, the effective Hamiltonian will lead to the population oscillating back and forth between $|1, 0\rangle$ and $|2, 0\rangle$ as described in section V (i.e. double-well dynamics).

If we follow the same procedure except for the manifold containing states of the form $|N_0, 1, N_1\rangle$, then we will find that the coupling terms are the same as above except multiplied by an extra factor of $(U - \hbar\Delta)/(U + \hbar\Delta)$, where U is the interaction energy between two $|1, -1\rangle$ atoms in the same lattice site. We therefore see that by choosing $\hbar\Delta = U$ there will be no coupling between different states in this manifold.

In section V, we considered $N_0 = 4N/5$, and $N_1 = N/5$. If we begin with no atoms in $|1, -1\rangle$ (i.e. our qubit is in the $|\downarrow\rangle$ state), then population will oscillate back and forth between $|1, 0\rangle$ and $|2, 0\rangle$. If instead we begin with one atom in $|1, -1\rangle$ (our qubit is $|\uparrow\rangle$), then there will be no population transfer.

Appendix F: Protocol to realize a $\sqrt{\text{SWAP}}$ gate

In this appendix, we describe how a $\sqrt{\text{SWAP}}$ gate could be realized without relying on the BEC to mediate the interaction.

IA beams are used to simultaneously address two qubits in the lattice, and the Ω_1 field is turned on to connect $|1, -1\rangle$ and $|2, 0\rangle$ with a large single-photon detuning, Δ (see Fig. 6). Since $|2, 0\rangle$ should be empty, in the limit $\Delta \gg \Omega_1$ this allows single atoms to jump between the two addressed lattice sites.

Given that $|\downarrow\rangle$ corresponds to an empty lattice site and $|\uparrow\rangle$ corresponds to a filled one, the effective Hamiltonian

describing this process is given by

$$H_{\text{eff}} = \begin{pmatrix} |\downarrow\downarrow\rangle \\ |\downarrow\uparrow\rangle \\ |\uparrow\downarrow\rangle \\ |\uparrow\uparrow\rangle \end{pmatrix} \begin{pmatrix} \hbar\omega_0 & & & \\ 0 & \hbar\omega_1 & & \\ 0 & -\hbar\Omega & \hbar\omega_2 & \\ 0 & 0 & 0 & \hbar\omega_3 \end{pmatrix}, \quad (\text{F1})$$

where each ω is the energy of the corresponding Fock state calculated using the first three terms of Eq. (4), and

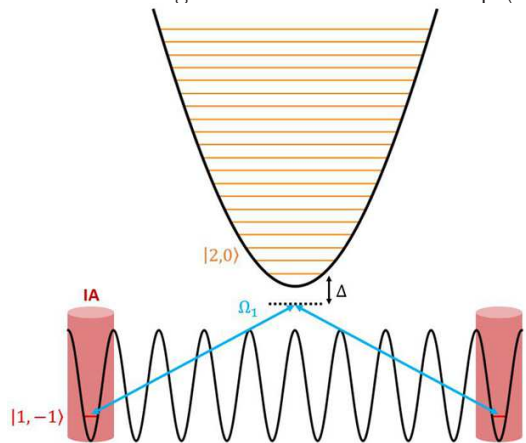


FIG. 6. Energy levels and fields involved in realizing a $\sqrt{\text{SWAP}}$ gate. Ω_1 is a MW field that connects $|1, -1\rangle$ and $|2, 0\rangle$ with single-photon detuning Δ . The beams used to address individual lattice sites are shown in red. The lowest Bloch band for the lattice is shown in red, and the first 20 (nondegenerate) 3D HO levels are shown in orange.

Ω is the effective coupling strength calculated from the last term of Eq. (4) following [68]. To realize a $\sqrt{\text{SWAP}}$ gate using Eq. (F1), a $\pi/2$ pulse between $|\downarrow\uparrow\rangle$ and $|\uparrow\downarrow\rangle$ is required, followed by a phase shift operation.

Due to the fact that $\omega_{\text{HO}} < \Delta$, the coupling between the Wannier wavefunctions and the excited spatial modes of the harmonic trap need to be taken into account to estimate Ω . We consider coupling qubits that are maximally far apart in the 3D lattice, with a free space Rabi frequency of $\tilde{\Omega}_1 = 2\pi \times 159$ kHz, and a single-photon detuning of $\Delta = 165$ kHz. After including first 20 nondegenerate levels (corresponding to 2,870 states) of the 3D HO, we obtain $\Omega = 2\pi \times 0.748$ Hz and a pulse length of 167 ms. With these parameters, we find that the estimated error is below 0.001.

-
- [1] M. A. Nielsen and I. L. Chuang, *Quantum Computation and Quantum Information* (Cambridge University Press, Cambridge, 2010).
 [2] G. K. Brennen, C. M. Caves, P. S. Jessen, and I. H. Deutsch, *Phys. Rev. Lett.* **82**, 1060 (1999).

- [3] D. Jaksch, H.-J. Briegel, J. I. Cirac, C. W. Gardiner, and P. Zoller, *Phys. Rev. Lett.* **82**, 1975 (1999).
 [4] D. S. Weiss and M. Saffman, *Physics Today* **70** (2017).
 [5] A. Negretti, P. Treutlein, and T. Calarco, *Quantum Information Processing* **10**, 721 (2011).

- [6] P.-I. Schneider and A. Saenz, *Phys. Rev. A* **85**, 050304 (2012).
- [7] J. Mompart, K. Eckert, W. Ertmer, G. Birkl, and M. Lewenstein, *Phys. Rev. Lett.* **90**, 147901 (2003).
- [8] A. Lengwenus, J. Kruse, M. Volk, W. Ertmer, and G. Birkl, *Applied Physics B* **86**, 377 (2007).
- [9] E. Brion, L. H. Pedersen, M. Saffman, and K. Mølmer, *Phys. Rev. Lett.* **100**, 110506 (2008).
- [10] I. I. Beterov, D. B. Tretyakov, V. M. Entin, E. A. Yakshina, I. I. Ryabtsev, C. McCormick, and S. Bergamini, *Phys. Rev. A* **84**, 023413 (2011).
- [11] M. D. Lukin, M. Fleischhauer, R. Cote, L. M. Duan, D. Jaksch, J. I. Cirac, and P. Zoller, *Phys. Rev. Lett.* **87**, 037901 (2001).
- [12] M. Anderlini, P. J. Lee, B. L. Brown, J. Sebby-Strabley, W. D. Phillips, and J. V. Porto, *Nature* **448**, 452 (2007).
- [13] M. Schlosser, J. Kruse, C. Gierl, S. Teichmann, S. Tichelmann, and G. Birkl, *New Journal of Physics* **14**, 123034 (2012).
- [14] J. Gelhausen, M. Buchhold, A. Rosch, and P. Strack, *SciPost Phys.* **1**, 004 (2016).
- [15] S. Welte, B. Hacker, S. Daiss, S. Ritter, and G. Rempe, *Phys. Rev. X* **8**, 011018 (2018).
- [16] L. Banchi, A. Bayat, P. Verrucchi, and S. Bose, *Phys. Rev. Lett.* **106**, 140501 (2011).
- [17] D. Jaksch, J. I. Cirac, P. Zoller, S. L. Rolston, R. Côté, and M. D. Lukin, *Phys. Rev. Lett.* **85**, 2208 (2000).
- [18] M. Saffman, T. G. Walker, and K. Mølmer, *Rev. Mod. Phys.* **82**, 2313 (2010).
- [19] H. Levine, A. Keesling, G. Semeghini, A. Omran, T. T. Wang, S. Ebadi, H. Bernien, M. Greiner, V. Vuletić, H. Pichler, and M. D. Lukin, *Phys. Rev. Lett.* **123**, 170503 (2019).
- [20] M. Morgado and S. Whitlock, *AVS Quantum Science* **3**, 023501 (2021), <https://doi.org/10.1116/5.0036562>.
- [21] W. S. Bakr, J. I. Gillen, A. Peng, S. Fölling, and M. Greiner, *Nature* **462**, 74 (2009).
- [22] K. D. Nelson, X. Li, and D. S. Weiss, *Nature Physics* **3**, 556 (2007).
- [23] T.-Y. Wu, A. Kumar, F. Giraldo, and D. S. Weiss, *Nature Physics* **15**, 538 (2019).
- [24] N. Lorenz, L. Festa, L.-M. Steinert, and C. Gross, *SciPost Phys.* **10**, 052 (2021).
- [25] Z.-B. Chen and Y.-D. Zhang, *Phys. Rev. A* **65**, 022318 (2002).
- [26] L. Tian and P. Zoller, *Phys. Rev. A* **68**, 042321 (2003).
- [27] K. T. Kapale and J. P. Dowling, *Phys. Rev. Lett.* **95**, 173601 (2005).
- [28] T. Byrnes, K. Wen, and Y. Yamamoto, *Phys. Rev. A* **85**, 040306 (2012).
- [29] D. Aghamalyan, N. T. Nguyen, F. Auksztol, K. S. Gan, M. M. Valado, P. C. Condylis, L.-C. Kwek, R. Dumke, and L. Amico, *New Journal of Physics* **18**, 075013 (2016).
- [30] W. Dubosclard, S. Kim, and C. L. Garrido Alzar, *Commun. Phys.* **4**, 35 (2021).
- [31] R. Yamamoto, J. Kobayashi, K. Kato, T. Kuno, Y. Sakura, and Y. Takahashi, *Phys. Rev. A* **96**, 033610 (2017).
- [32] M. R. Andrews, M.-O. Mewes, N. J. van Druten, D. S. Durfee, D. M. Kurn, and W. Ketterle, *Science* **273**, 84 (1996), <https://www.science.org/doi/pdf/10.1126/science.273.5271.84>.
- [33] M. Saba, T. A. Pasquini, C. Sanner, Y. Shin, W. Ketterle, and D. E. Pritchard, *Science* **307**, 1945 (2005), <https://www.science.org/doi/pdf/10.1126/science.1108801>.
- [34] J. M. Higbie, L. E. Sadler, S. Inouye, A. P. Chikkatur, S. R. Leslie, K. L. Moore, V. Savalli, and D. M. Stamper-Kurn, *Phys. Rev. Lett.* **95**, 050401 (2005).
- [35] Y. Colombe, T. Steinmetz, G. Dubois, F. Linke, D. Hunger, and J. Reichel, *Nature* **450**, 272 (2007).
- [36] D. McKay and B. DeMarco, *New Journal of Physics* **12**, 055013 (2010).
- [37] I. de Vega, D. Porras, and J. Ignacio Cirac, *Phys. Rev. Lett.* **101**, 260404 (2008).
- [38] C. Navarrete-Benlloch, I. de Vega, D. Porras, and J. I. Cirac, *New Journal of Physics* **13**, 023024 (2011).
- [39] R. Grimm, M. Weidemüller, and Y. B. Ovchinnikov (Academic Press, 2000) pp. 95 – 170.
- [40] C. Weitenberg, M. Endres, J. F. Sherson, M. Cheneau, P. Schauß, T. Fukuhara, I. Bloch, and S. Kuhr, *Nature* **471**, 319 (2011).
- [41] J. H. Lee, E. Montano, I. H. Deutsch, and P. S. Jessen, *Nature Communications* **4**, 2027 (2013).
- [42] D. Barredo, V. Lienhard, S. de Léséleuc, T. Lahaye, and A. Browaeys, *Nature* **561**, 79 (2018).
- [43] A. Kumar, T.-Y. Wu, F. Giraldo, and D. S. Weiss, *Nature* **561**, 83 (2018).
- [44] T. Grünzweig, A. Hilliard, M. McGovern, and M. F. Andersen, *Nature Physics* **6**, 951 (2010).
- [45] A. Vepsäläinen, R. Winik, A. H. Karamlou, J. Braumüller, A. D. Paolo, Y. Sung, B. Kannan, M. Kjaergaard, D. K. Kim, A. J. Melville, B. M. Niedzielski, J. L. Yoder, S. Gustavsson, and W. D. Oliver, *Nature Communications* **13**, 1932 (2022).
- [46] L. E. de Clercq, R. Oswald, C. Flühmann, B. Keitch, D. Kienzler, H.-Y. Lo, M. Marinelli, D. Nadlinger, V. Negnevitsky, and J. P. Home, *Nature Communications* **7**, 11218 (2016).
- [47] Q. Guo, S.-B. Zheng, J. Wang, C. Song, P. Zhang, K. Li, W. Liu, H. Deng, K. Huang, D. Zheng, X. Zhu, H. Wang, C.-Y. Lu, and J.-W. Pan, *Phys. Rev. Lett.* **121**, 130501 (2018).
- [48] P. Xue and Y.-F. Xiao, *Phys. Rev. Lett.* **97**, 140501 (2006).
- [49] R. S. Gupta, L. C. G. Govia, and M. J. Biercuk, *Phys. Rev. A* **102**, 042611 (2020).
- [50] P. Öhberg and S. Stenholm, *Phys. Rev. A* **59**, 3890 (1999).
- [51] M.-S. Chang, Q. Qin, W. Zhang, L. You, and M. S. Chapman, *Nature Physics* **1**, 111 (2005).
- [52] Y. Kawaguchi and M. Ueda, *Physics Reports* **520**, 253 (2012), spinor Bose–Einstein condensates.
- [53] N. Irikura, Y. Eto, T. Hirano, and H. Saito, *Phys. Rev. A* **97**, 023622 (2018).
- [54] A. Widera, F. Gerbier, S. Fölling, T. Gericke, O. Mandel, and I. Bloch, *New Journal of Physics* **8**, 152 (2006).
- [55] F. Dalfvo, S. Giorgini, L. P. Pitaevskii, and S. Stringari, *Rev. Mod. Phys.* **71**, 463 (1999).
- [56] J. Javanainen, *Phys. Rev. A* **54**, R3722 (1996).
- [57] D. Jaksch, C. Bruder, J. I. Cirac, C. W. Gardiner, and P. Zoller, *Phys. Rev. Lett.* **81**, 3108 (1998).
- [58] H. Miyake, G. A. Siviloglou, C. J. Kennedy, W. C. Burton, and W. Ketterle, *Phys. Rev. Lett.* **111**, 185302 (2013).

- [59] Y. Wang, X. Zhang, T. A. Corcovilos, A. Kumar, and D. S. Weiss, *Phys. Rev. Lett.* **115**, 043003 (2015).
- [60] A. Barenco, C. H. Bennett, R. Cleve, D. P. DiVincenzo, N. Margolus, P. Shor, T. Sleator, J. A. Smolin, and H. Weinfurter, *Phys. Rev. A* **52**, 3457 (1995).
- [61] S. J. M. Kuppens, K. L. Corwin, K. W. Miller, T. E. Chupp, and C. E. Wieman, *Phys. Rev. A* **62**, 013406 (2000).
- [62] N. Schlosser, G. Reymond, and P. Grangier, *Phys. Rev. Lett.* **89**, 023005 (2002).
- [63] C. Sias, H. Lignier, Y. P. Singh, A. Zenesini, D. Ciampini, O. Morsch, and E. Arimondo, *Phys. Rev. Lett.* **100**, 040404 (2008).
- [64] B. Merkel, K. Thirumalai, J. E. Tarlton, V. M. Schäfer, C. J. Ballance, T. P. Harty, and D. M. Lucas, *Review of Scientific Instruments* **90**, 044702 (2019), <https://doi.org/10.1063/1.5080093>.
- [65] P. Würtz, T. Langen, T. Gericke, A. Koglbauer, and H. Ott, *Phys. Rev. Lett.* **103**, 080404 (2009).
- [66] T. Weber, J. Herbig, M. Mark, H.-C. Nägerl, and R. Grimm, *Phys. Rev. Lett.* **91**, 123201 (2003).
- [67] A. P. Chikkatur, Y. Shin, A. E. Leanhardt, D. Kielpinski, E. Tsikata, T. L. Gustavson, D. E. Pritchard, and W. Ketterle, *Science* **296**, 2193 (2002), <https://www.science.org/doi/pdf/10.1126/science.296.5576.2193>.
- [68] C. Cohen-Tannoudji, J. Dupont-Roc, and G. Grynberg, *Atom-photon interactions: Basic processes and applications* (Wiley, New York, 1988) Chap. Compliment B_1 —Description of the Effect of a Perturbation by an Effective Hamiltonian.